*Journal of Sound and Vibration* (2000) **235**(2), 281–297
doi:10.1006/jsvi.2000.2920, available online at http://www.idealibrary.com on IDEAL®

# A NOVEL INVESTIGATION OF THE OSCILLATORY FIELD OVER A TRANSPIRING SURFACE

JAMES T. BARRON

*Department of Mechanical Engineering, LAN Inc., Lee Park Center, 3141 Hood Street, Dallas, TX 75219, U.S.A. E-mail: jbarron@lan-inc.com*

WILLIAM K. VAN MOORHEM

*Mechanical Engineering Department, University of Utah, 2202 Merrill Engineering Building, Salt Lake City, UT 84112, U.S.A. E-mail: van@eng.utah.edu*

AND

JOSEPH MAJDALANI

*Department of Mechanical and Industrial Engineering, Marquette University, 1515 West Wisconsin Avenue, Milwaukee, WI 53233, U.S.A. E-mail: maji@mu.edu*

(*Received* 12 *March* 1999, *and in final form* 11 *February* 2000)

The flowfield character is investigated inside a long rectangular chamber in the presence of time-harmonic pressure waves. The chamber is designed with multiple interchangeable sections for the purpose of controlling the length and therefore the system's natural frequency. Pressure waves are induced externally at variable frequencies by means of a Scotch-yoke mechanism theoretically capable of imparting pure oscillatory motions. In characterizing the internal flowfield, velocity measurements are acquired inside a principal test section that can accommodate flat blocks of solid carbon dioxide (i.e., dry ice). As solid $CO_2$ sublimates, a flow of gaseous carbon dioxide is generated at the bottom of the principal section and enters the chamber in the transverse direction. The resulting generalized Stokes layer formed above the transpiring surface exhibits several features associated with oscillatory flows over impermeable surfaces, including an overshoot in the velocity amplitude in the vicinity of the transpiring wall known as Richardson's annular effect. Quantitative pressure and velocity measurements are in agreement with theoretical predictions obtained from recent models of the oscillatory field over transpiring surfaces. The acoustic Reynolds number based on the Stokes layer thickness increases linearly with increasing Scotch-yoke frequency except in the neighborhood of the system's natural frequency. Near resonance, a sharp non-linear increase in the acoustic Reynolds number is noted. Furthermore, both acoustic pressure and velocity amplitudes increase with the driving frequency in a manner that is consistent with current theories. Since the sublimation rate of dry ice can be expressed in a similar mathematical form to the regression rate at the burning surface of solid propellants, this experiment constitutes a cold flow simulation of the internal flowfield in solid rocket motors.



## 1. INTRODUCTION

Going back through available literature, only few experimental investigations are found that address the nature of the oscillatory flowfield over a transpiring surface. This may be attributed to the inherent difficulty in designing and measuring flow parameters in such

0022-460X/00/320281 + 17 $35.00/0 

unsteady environments in the absence of analytical formulations to help in the planning process. Motivation for such an experiment arose, not long ago, from the need to increase our understanding of the fluid dynamical coupling inside acoustically unstable rocket chambers. Here, resolving the corresponding flow features demands a careful assessment of the inherent coupling between gases injected inwardly and the oscillatory waves triggered by unsteady combustion.

In the hope of elucidating the nature of the resulting flowfield, an experimental investigation was conducted by Brown and co-workers [1–4]. They used nitrogen gas injection through uniformly sintered bronze plates inside a cylindrical chamber. In their facility, acoustic waves were generated from an external rotary valve that controlled the flow exiting the chamber. Brown's results verified the accuracy of the analytical model suggested by Culick [5] for the mean flowfield and also provided substantial data for the resulting acoustic field. Independently of Brown's work, a novel experimental facility was built by Ma [6–9] to simulate similar flowfield conditions in a rectangular chamber. The unique feature of Ma's experiment was that it employed the sublimation of carbon dioxide, a process that resembled the combustion of a propellant, in generating the $CO_2$ gas at what would become the chamber's "transpiring" wall.

The sublimation of solid $CO_2$ was chosen over previously used simulation techniques for several reasons. Although weaker, the dynamic behavior of the solid $CO_2$ is analogous to the behavior of actual propellant. In a rocket motor, increasing the pressure results in an increase in propellant burn rate and mass flow rate. Similarly, an increase in the pressure over the solid $CO_2$ results in an increase in the sublimation rate and therefore mass flow from the surface. This increase is due to the decrease in the heat of sublimation with increasing pressure. Other cold flow facilities usually simulate the combustion process by injecting gas through a porous wall. The pores must be choked to prevent acoustic energy from being lost into the wall. An increase in pressure above the porous wall results in either unchoking of the pores and decreasing the massflow or a constant mass flow rate if the pores remain choked. Neither of these results simulates actual propellant. An even more serious problem is the possibility that the injection process itself causes turbulence. The use of solid $CO_2$ eliminates the question of choking or not choking at the pores and makes it ideally suited for simulating the behavior of a solid rocket motor propellant.

Ma [7] measured pressure, velocity, and mass flow rates of the gaseous carbon dioxide as a function of frequency in his experiments. Unfortunately, the work by Ma had experimental difficulties in measuring acoustic pressure and velocity. The reason: he used, as a wave generator, a slider-crank mechanism consisting of a cylindrical piston, connecting rod, and crankshaft arrangement. Since the wave motion produced by a slider-crank mechanism is not purely sinusoidal, Ma's wave generator produced many harmonics that complicated the analysis of his acoustic data. Ma thought that turbulence occurred in his experiments. However, due to the complex acoustic waves and lack of statistical data, Ma's experiments did not have the capability to verify the occurrence of turbulence.

In the current work, the problems encountered in Ma's investigation will be alleviated first by changing the means of generating acoustic waves and second, by employing a reliable statistical data acquisition package. The first improvement is achieved by utilizing a Scotch-yoke mechanism to replace the slider-crank mechanism that was used previously.

Another purpose of this investigation is to compare experimental data to predictions derived from analytical models of the flowfield by Majdalani [10, 11].

To summarize, the purpose of this paper will be to discuss the design and subsequent results of an experimental investigation of the oscillatory velocity field over a transpiring surface. Such results are hoped to validate recent theoretical formulations. The advantages of using the current experimental set-up for the purpose of obtaining reliable data will be

stated along with a brief review of previously used approaches. The principal advantage of the current set-up is that it employs a Scotch-yoke mechanism to produce a more nearly pure harmonic motion, thus eliminating or minimizing undesired harmonic frequencies arising from the use of other driving mechanisms. The transpiring surface consists of sublimating dry ice and the working fluid is carbon dioxide. Experimental data sets will be compared and shown to be agreeable with recent analytical solutions for the velocity flowfield established in such an environment.

## 2. IMPROVED WAVE GENERATOR

Different mechanisms are used to produce the oscillatory motion: slider-crank, rotating valves, Scotch-yoke, etc. Schematics of two commonly used devices are furnished below (see Figure 1).

The piston position for a crankshaft-connecting rod system is given by the expression

$$x = r\cos(\omega t) + l\sqrt{1 - \left(\frac{r}{l}\right)^2 \sin^2(\omega t)}, \tag{1}$$

where $\omega$ is the circular frequency, $r$ the offset of the crankshaft throw, $l$ the length of the connecting rod, and $z \equiv r/l$ is small, generally about 1/4. When this motion is expressed in the form of Fourier series with the assumption of small values of $z$, one obtains

$$x = l(1 - \tfrac{1}{4}z^2 - \tfrac{3}{64}z^4 + \cdots) + r\cos(\omega t) + l(\tfrac{1}{4}z^2 - \tfrac{1}{16}z^4 + \cdots)\cos(2\omega t)$$
$$+ l(-\tfrac{1}{64}z^4 + \cdots)\cos(4\omega t) + \cdots.$$

In reality, terms with $z$ to powers higher than four can be ignored for typical devices. This series clearly points out that only odd harmonics of the fundamental frequency should be seen. In actuality, all the harmonics are seen, not only the odd harmonics. This is due to non-ideal piston motion caused by the looseness in the bearings [7] and to the fundamental non-linear nature of fluid motions. If all the harmonics are present, then a solution for the gas velocity $u'$ in a tube can be expressed in the form

$$u' = \frac{u_1}{\sin(kl)}\sin[k(L-x)]\cos(\omega t) + \frac{u_2}{\sin(2kl)}z\sin[2k(L-x)]\cos(2\omega t)$$
$$+ \frac{u_3}{\sin(3kl)}z^2\sin[3k(L-x)]\cos(3\omega t) + \mathrm{O}(z^3), \tag{3}$$

where $u_1$, $u_2$, and $u_3$ are constants [7].

Resonance or acoustic amplification will hence occur when the piston driving frequency is $1/m$ of the fundamental natural frequency of the tube, since now $\sin(mkl) = 0$ at resonance. These frequencies are

$$f_0 = a_0/(2L); \quad f_m = a_0/(2mL); \quad m = 1, 2, \cdots. \tag{4}$$

In the higher fractional cases, since the piston amplitude is smaller than the fundamental one, a much weaker excitation is observed. Theoretically, resonance can also occur when the piston is running at one-fourth (or even smaller fractions) of the chamber's natural frequency: these resonant peaks are usually negligible due to the weak driving amplitude of

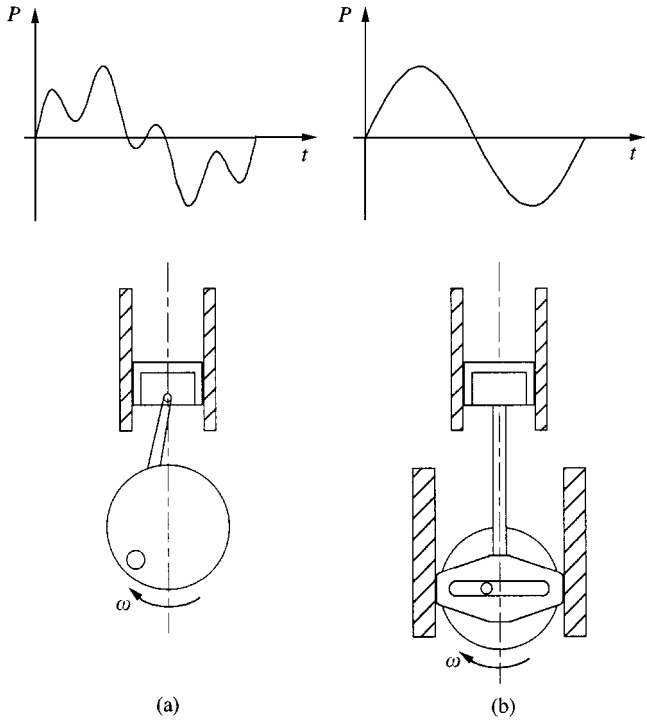


Figure 1. Pressure versus time for (a) piston with slider-crank configuration, and (b) piston with Scotch-yoke configuration.

the order of $z$ to the third or higher power. Thus for realistic values of $z$, one would expect large amplitudes around driving frequencies of $f = a_0/(4L)$, $a_0/(3L)$, $a_0/(2L)$, and $a_0/L$, etc.

As shown in Figure 1, the slider-crank mechanism does not produce a pure sinusoidal piston motion. Since the piston movement is not purely sinusoidal, many harmonics are introduced into the acoustic velocity and pressure fields. The sketch of pressure versus time demonstrates the harmonics that complicate the acoustic data when using the slider-crank arrangement. The added harmonics in the acoustic data make it very difficult to undertake meaningful statistical and Fourier analyses for determining the occurrence of turbulence. As shown by a plot of pressure versus time in Figure 1, the Scotch-yoke provides, in theory, a pure sinusoidal piston motion. Such motion leads to improved control over the fundamental frequency and harmonics of the oscillating pressure and velocity fields.

## 3. EXPERIMENTAL FACILITY

### 3.1. DESCRIPTION

The Solid Carbon Dioxide Simulation Facility is a "cold flow" (nonreactive) facility (Figure 2). The use of solid carbon dioxide (dry ice) is to simulate the internal flowfield of a solid propellant rocket motor. By using dry ice as the simulated propellant, it is possible to focus on the fluid mechanics of the acoustic instability problem by separating the fluid mechanics from the combustion of actual propellant. The flow chamber has a square cross section with an inside dimension of $7{\cdot}62 \times 7{\cdot}62$ cm. The flow chamber consists of eight

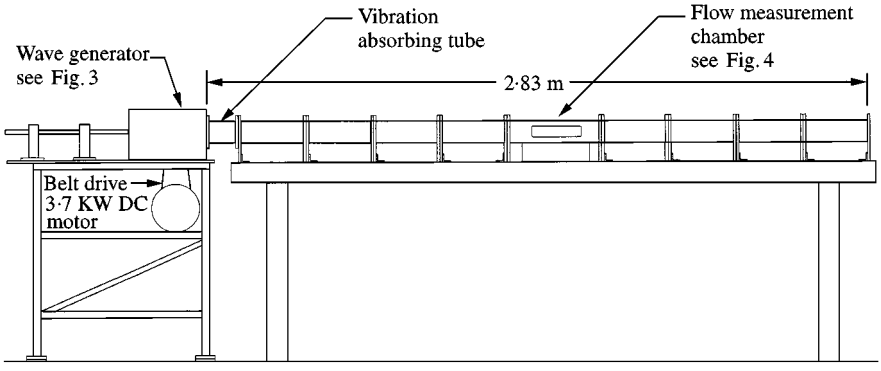


Figure 2. Experimental apparatus.

interchangeable sections, a test section used to hold the dry ice, and a vibration isolating section. The entire flow chamber is bolted to a heavy granite table to minimize vibration. The interchangeable sections make it possible to vary the test section location, chamber length and system resonant frequency. For these experiments, the length was held constant at 2·83 m corresponding to a resonant frequency of 49 Hz at a temperature of 27°C.

### 3.2. EXPERIMENTAL CONFIGURATIONS

Two types of experiments were performed. The first set of experiments were carried out without dry ice in the flow chamber at driving frequencies ranging between 2·3 and 44·8 Hz. The second set of experiments were carried out with dry ice in the flow chamber to simulate propellant combustion at driving frequencies ranging between 2·2 and 50·8 Hz. For all experiments, the chamber was initially purged with room-temperature $CO_2$ (gas) to remove the air.

### 3.3. WAVE GENERATOR

A wave generator located at one end of the flow chamber is used to produce an acoustic environment inside the chamber. A mechanical driving system based on a Scotch-yoke mechanism was designed and built for that purpose (see Figure 3). The wave generator has a volumetric displacement of 232 $cm^3$ and is driven by a 3·7 kW variable-speed DC motor. The connecting rod has a linear motion and is supported by two linear bearings. In addition, it is harnessed rigidly to the piston and the Scotch-yoke. The Scotch-yoke also has a linear motion and has a slot for crankshaft travel. This set-up leads, in theory, to a pure sinusoidal piston motion. The flow chamber is isolated from vibration caused by the wave generator and motor by using both a vibration isolating tube between the wave generator and the flow chamber, and neoprene pads under the feet of the chamber support structure.

### 3.4. PRINCIPAL TEST SECTION

The center section of the flow chamber is a 43·2 cm long test section (see Figure 2). The test section is placed near the center of the chamber where the acoustic velocity antinode (maximum velocity) coincides with the location of a pressure node (pressure minimum) for

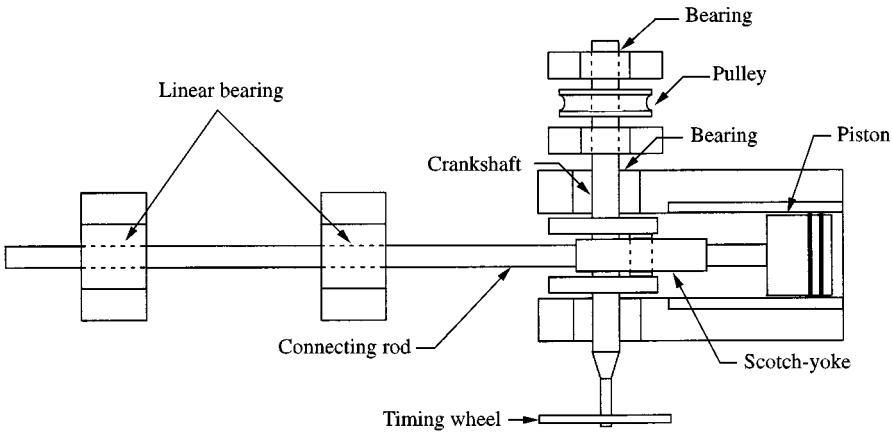


Figure 3. Wave generator.

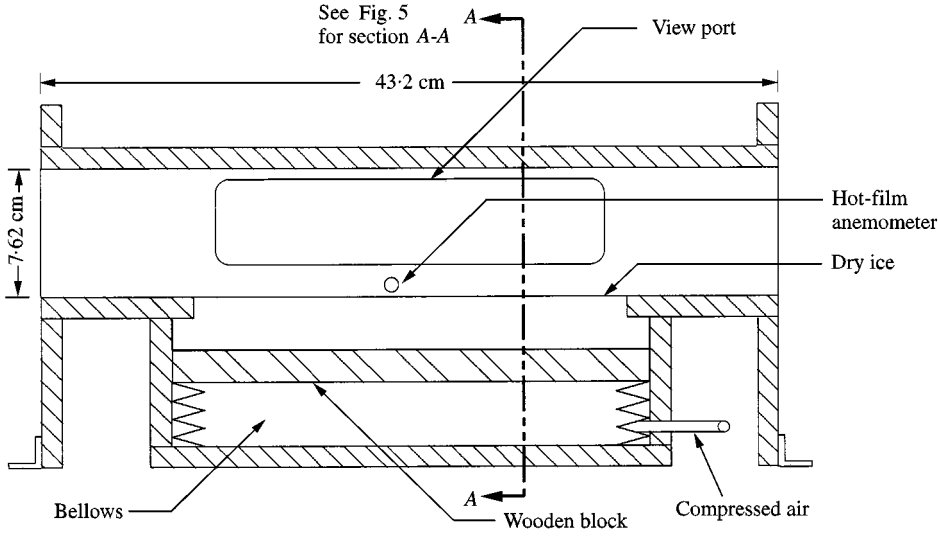


Figure 4. Flow measurement chamber.

a standing wave. This set-up minimizes any pressure dependence in the dry ice sublimation. Figure 4 shows a section view of the test section. Solid carbon dioxide (dry ice) is used in the test section to simulate solid propellant rocket motor characteristics. The sublimation of the solid $CO_2$ into gaseous carbon dioxide simulates the burning of the propellant. The solid $CO_2$ is a commercial dry ice block approximately 30 cm long, 5 cm deep, and 7·62 cm in width which is equal to the width of the test section. The dry ice rests on a wooden block and a bellows is used to maintain the top of the dry ice at the same level as the bottom of the test section. The bellows pushes the dry ice with a constant supply air pressure of 3 psig. The bellows supply pressure is sufficiently large to eliminate significant vibration of the dry ice block due to acoustic pressure oscillations on the top dry ice surface. The dry ice can be replaced with a fitted aluminum plate that makes the investigation of the flowfield without

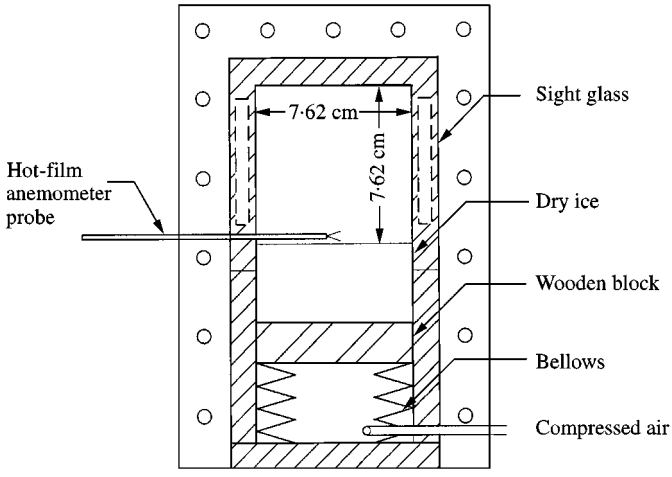


Figure 5. Section A-A: flow measurement section.

side-wall injection possible. Glass view ports are located on either side of the test section to facilitate visual flow monitoring. The velocity of the gas near the surface of the dry ice can be measured by hot-film anemometry.

### 3.5. HOT FILM ANEMOMETRY

A hot-film anemometer is mounted in the test section as shown by section A-A in Figure 5. The hot film probe is centered above the dry ice and is located approximately 8 mm above the surface of the dry ice. The hot film probe is mounted perpendicularly to the dry ice surface. The advantage of using a hot-film over a hot wire is that the hot film has a faster response to velocity changes, a feature that is needed in acquiring turbulent velocity data. In fact, assessment of turbulence constitutes another facet of this investigation that is hoped to be addressed in a forthcoming article.

### 3.6. PRESSURE MEASUREMENT

Pressure oscillations in the flow chamber can also be measured. A pressure transducer can be mounted at various locations in the chamber to record the pressure oscillations. For these experiments, the pressure transducer was located at the end of the flow chamber opposing the wave generator where maximum pressure is observed.

By comparison with formerly used wave generators, the larger volumetric displacement of the Scotch-yoke (262 $cm^3$) results in a larger pressure amplitude than in previous work. Increasing the pressure over the solid $CO_2$ reduces its heat of sublimation. This results in an increase in the sublimation rate and mass flow from the surface. Ma [7] used an infrared light above the dry ice to increase the sublimation rate. The infrared light also heated the hot-film probe and resulted in zero bridge voltage and electronic oscillations in the anemometer control circuit. This was detrimental to velocity measurements. By increasing the oscillating pressure amplitude instead of using an infrared heat lamp, velocity measurements with the hot-film probe were facilitated.

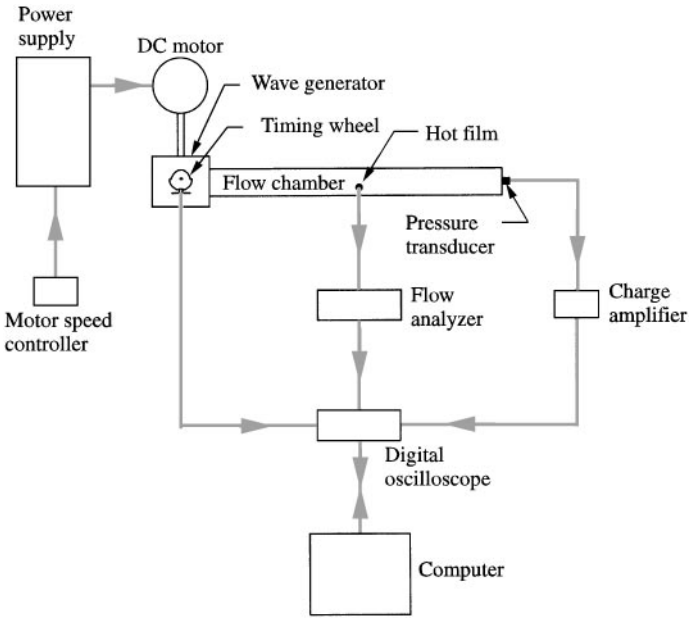


Figure 6. Experimental system.

### 3.7. INSTRUMENTATION

The instrumentation used to acquire velocity and pressure data from the Solid Carbon Dioxide Simulation Facility is described in this section and is shown schematically in Figure 6. An acoustic flowfield is produced in the flow chamber by a wave generator. The wave generator is powered by a 3·7 kW DC motor and power supply. The driving frequency of the piston is controlled by a potentiometer connected to the power supply. A pressure transducer (Kistler model 606L) is used to monitor pressure oscillations generated in the flow chamber. A charge amplifier (PCB model 464A) converts signals from the piezoelectric pressure transducer to standardized voltage signals compatible with readout instruments. The resultant voltage signal then goes to a digital oscilloscope (HP model 54501A) where the pressure data is digitized. The computer gets the pressure data from the oscilloscope and saves the data for analysis. A low-noise, constant temperature hot-film probe (TSI model 1210-60) is used to measure velocity oscillations generated in the flow chamber. The flow analyzer (Intelligent Flow Analyzer model 100) converts the current from the sensor to a voltage proportional to velocity. The flow signal conditioner also filters unwanted noise and amplifies the signal. The analog velocity signal goes from the flow analyzer to the oscilloscope where it is digitized. The computer receives and stores the velocity data from the oscilloscope.

### 3.8. OPERATION

In order to perform statistical analyses, multiple acoustic velocity and pressure data sets at a given frequency have to be collected with the same starting point in the mechanical driving cycle. A timing wheel and a timing signal are employed to consistently begin the collection of each data set at the same point in the mechanical driving cycle (see Figure 7). The timing wheel is mounted on the crankshaft as shown by Figure 3. The outer portion of

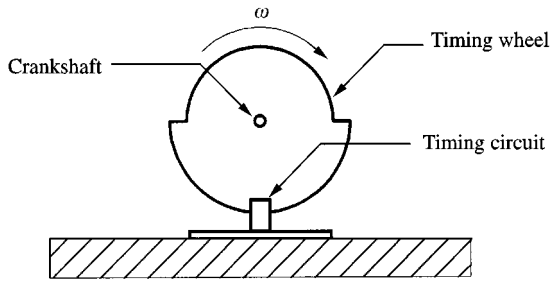


Figure 7. Section A-A: timing wheel.

the timing wheel is centered in a slot which has a light sensor. The light sensor is blocked when the large radius portion of the timing wheel rotates through the slot as shown in Figure 7. When the timing wheel rotates so that the large radius portion of the timing wheel is not in the slot, the light is not blocked and the timing circuit is closed. The resulting timing signal is a square wave. Data are collected when the computer sends a signal to the oscilloscope to start collecting data and the timing wheel rotates to the point where the timing circuit is closed. Acoustic data (either velocity or pressure) are then collected at the oscilloscope and sent to the computer to be stored. The pressure and velocity data acquired in the experiments are Fourier analyzed to demonstrate the reliability of the driving mechanism.

In order to complete a statistical analysis of the data, between 10 and 15 data sets are collected at a given piston driving frequency. The data sampling frequency is varied with frequency of the driving piston. Each data set consists of 512 data points which are collected during a time period corresponding to approximately two driving piston cycles. Since the piston frequency is varied between 2·2 and 50·8 Hz, the sampling frequency varies between 512 and 10,240 Hz.

Calibration of the hot-film anemometer is extremely important. The sensing elements are delicate mechanically and analog output signals have a tendency to drift. To compensate, frequent checks of probe calibration are necessary. Hot-film anemometers are repeatable but accuracy is a function of how closely the calibration conditions are being reproduced in the flow to be measured. To that end, calibration was performed before each data set was acquired. A flow generator with a plenum chamber and an ASME nozzle were used to get a known air velocity for calibration. The nozzle exit velocity was determined from Bernoulli's equation. An assumption that the static pressure of the air exiting the nozzle is equal to the outside atmospheric pressure was used. A calibration relationship was determined between known velocity and bridge voltage with the hot-film probe located at the nozzle exit. The relationship is non-linear (approximately a 1/4 power relation). Figure 8 shows a typical hot-film calibration curve. In Figure 8, the horizontal axis is the known air velocity from the ASME nozzle. The vertical axis represents the voltage output from the hot-film anemometer.

## 4. SOME THEORETICAL BACKGROUND

### 4.1. ON THE STOKES LAYER

Due to the prevalent oscillatory motion, the boundary layer formed over the surface is of the Stokes type. The Stokes layer over a hard wall denotes the region where viscous and

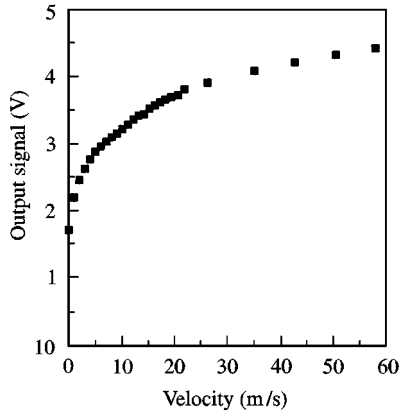


Figure 8. Calibration curve of a hot-film anemometer.

rotational flow conditions persist due to the presence of solid boundaries [12]. The thickness of this region is determined by viscosity and frequency and does not grow with time or distance. The idea behind this characteristic length can be clarified by looking at the case known as Stokes' second problem [12]. In that problem, Stokes [13] considers an inertial, viscous, incompressible and two-dimensional fluid in contact with an infinitely long plate that is in oscillatory motion. The velocity field is readily found to be

$$u(y,t) = U_0 \mathrm{e}^{-\sqrt{(\omega/2\nu)}y} \cos\left[\omega\left(t - \frac{y}{\sqrt{2\omega\nu}}\right)\right] \tag{5}$$

where $U_0$ denotes the amplitude of velocity oscillations, $y$ is the distance above the wall, and $\nu$ is the kinematic viscosity.

While the frequency of oscillations is given by $f = \omega/(2\pi)$, the speed of wave propagation is $\sqrt{2\omega\nu}$; this indicates that larger frequency or kinematic viscosity lead to larger propagation rate of disturbances. At a sufficiently large distance from the solid boundary, the flow can be considered to be unaffected by the presence of the wall. Stokes [13] introduces a length scale $\delta_{St} = 2\sqrt{2\nu/\omega}$ such that when the distance from the wall is equal to $\delta_{St}$, the amplitude of the velocity reaches 13·5% of its initial value. Other researchers define the Stokes boundary layer thickness to be equal to one wavelength, $\lambda_{St} = 2\pi\sqrt{2\nu/\omega}$, for which the rotational velocity amplitude reduces to 0·2% of its initial value. Evidently, a layer that scales with $\delta_{St} = \sqrt{2\nu/\omega}$ is indicative of the domain where the flow senses the presence of solid boundaries. This scale is analogous to the boundary layer thickness encountered in non-periodic flows.

### 4.2. ON THE ACOUSTIC REYNOLDS NUMBER

Due to the important role that the Stokes layer plays in periodic flows, several so-called "acoustic Reynolds numbers" based on some form of $\delta$ have been introduced in the past. In fact, most Reynolds numbers found in the literature differ from one another by a pure constant. It appears that the most popular three are $Re_\delta$, $Re_A$, and $A$. These are defined

as

$$Re_\delta = \frac{U_0\delta}{v} = \frac{U_0\sqrt{2}}{\sqrt{\omega v}} = \frac{A}{\sqrt{2}} = \frac{Re_A}{\sqrt{\pi}}, \tag{6}$$

$$Re_A = \frac{U_0}{\sqrt{fv}} = \frac{U_0\sqrt{2\pi}}{\sqrt{\omega v}} = \sqrt{\frac{\pi}{2}}A = \sqrt{\pi}\,Re_\delta, \tag{7}$$

$$A = \frac{2U_0}{\sqrt{\omega v}} = \sqrt{2\pi}\frac{U_0}{\sqrt{\omega v}} = \sqrt{\frac{2}{\pi}}Re_A = \sqrt{2}Re_\delta \tag{8}$$

It is recommended that a unifying symbol be articulated to facilitate data comparison from diverse experiments. In this article, the acoustic Reynolds number $Re_A$ shall be used.

## 5. RESULTS AND DISCUSSION

### 5.1. VELOCITY MEASUREMENTS AND SPECTRAL ANALYSIS

Two oscillatory flow conditions are investigated in the central chamber purged with $CO_2$ gas. The two conditions are: (1) oscillatory flow with side-wall injection and (2) oscillatory flow without side-wall injection. Experiments with side-wall injection are performed for driving frequencies between 2·2 and 50.8 Hz for which $83 < Re_A < 2150$. The driving frequencies for experiments with sidewall injection include 2·2, 7·0, 11·8, 15·5, 20.0, 24·7, 30.4, 35·5, 41·2, and 50·8 Hz. Experiments without sidewall injection are performed for driving frequencies between 2·3 and 44·8 Hz for which $55 < Re_A < 500$. The smaller range of $Re_A$ (with no dry ice) can be attributed to the reduced acoustic velocity amplitude when injection is suppressed. The driving frequencies for experiments without sidewall injection include 2·3, 6·3, 10·6, 14·9, 21·0, 24·6, 29·0, 36·4, 41·5, and 44·8 Hz. In both instances, typical velocity and pressure traces are shown in Figure 9 (for $f = 2{\cdot}2$ and 2·3 Hz with and without dry ice respectively). Note the dramatic increase (doubling) of the maximum acoustic velocity in the experiment with sidewall injection. Clearly, velocity fluctuations in the laminar case have small amplitudes that are larger near the wall. This increase is more substantial when the wall is made permeable.

A spectral analysis is now performed on the acoustic velocity and pressure data using a fast Fourier transform (FFT) algorithm. The power spectral density (PSD) of the various frequencies present in the acoustic oscillations is important in determining the relationship between frequency and flow phenomena such as turbulence. The reason is this. For a purely sinusoidal driver, a velocity peak would be expected to occur in the laminar flow spectrum at the driving frequency only. The intrinsic nonlinear behavior of fluid flow may, however, generate harmonics and sub-harmonics. If a slider-crank driver is used, the harmonics of the driving frequency will be significantly increased. The spurious presence of several peaks (at integral multiples of the driving frequency) can complicate data interpretation by giving a false indication of a turbulent flow spectrum. This problem is alleviated, of course, when a Scotch-yoke is used. For illustrative purposes, Figure 10 is used to compare PSD plots for experiments with (a) Scotch-yoke and (b) slider-crank driving mechanisms. Both with and without dry ice, the presence of a peak (at the driving frequency) in Figure 10(a) is in agreement with acoustic theory. This cannot be said of Figure 10(b) where the addition of multiple peaks precludes a meaningful assessment of the spectral content. From this typical example, the advantage of using a Scotch-yoke is clearly seen.

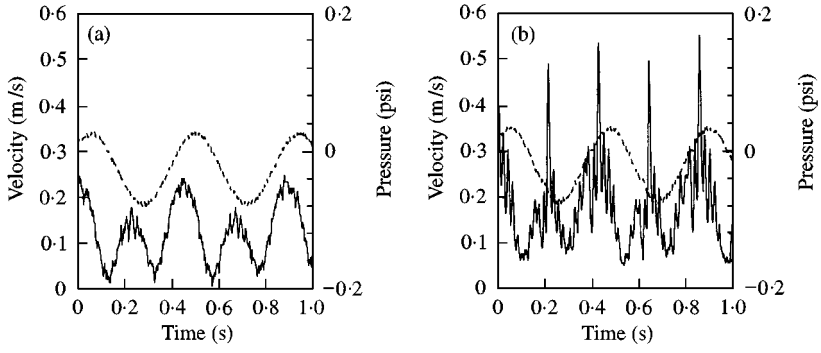


Figure 9. Velocity (——) and pressure (- - -) traces obtained from hot-film and pressure measurements. Here, the hot film is located 8 mm above the wall and $f = 2{\cdot}2$ Hz. The two cases are for (a) impermeable and (b) transpiring walls. Note the increase in acoustic velocity amplitude with the addition of sidewall injection.

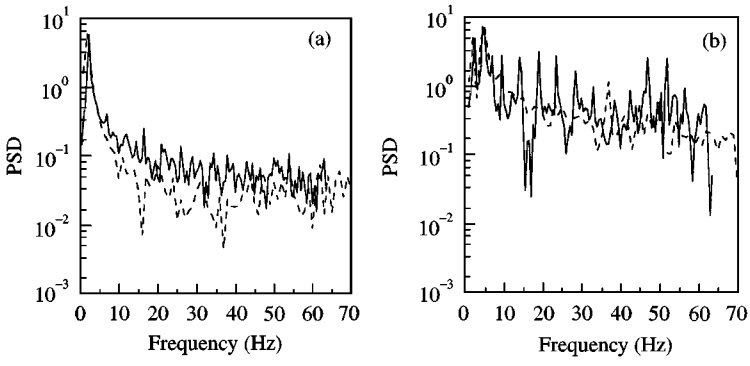


Figure 10. Spectral analysis (power spectral density) of pressure data with (——) and without (- - -) sidewall injection using (a) Scotch-yoke and (b) slider-crank driving mechanisms.

In our experiment, the fundamental frequency of the flow chamber is determined using linear acoustic theory. In this, we follow Ma [7] who examined the spectral output of pressure signals at two different locations in the flow chamber while operating a wave generator at one-half of the chamber's fundamental frequency. By knowing the ratio of the pressure amplitudes for the chamber's fundamental frequency (the first harmonic of the piston motion in this case) and the distance between the two pressure transducers, the speed of sound can be calculated using linear theory. The speed of sound is thus found to be 279·5 m/s with dry ice in the test section and 274·9 m/s without dry ice. The fundamental frequency of the flow chamber for these experiments is 47 Hz with sidewall injection from dry ice. The fundamental frequency increases to 49 Hz for experiments without sidewall injection.

The hot-film anemometer used to measure velocity cannot differentiate the direction of flow. Therefore, the output signal for all of the velocity measurements is a rectified signal. Because the velocity signal is rectified, the reader must be cautioned that the spectrum analysis shows peaks at both the driving frequency and double the driving frequency.

Figure 11 shows the relationship between $Re_A$ and driving frequency. $Re_A$ increases linearly with increasing frequency up to approximately 30 Hz and then increases more rapidly as the driving frequency approaches the chamber's resonant frequency. An increase

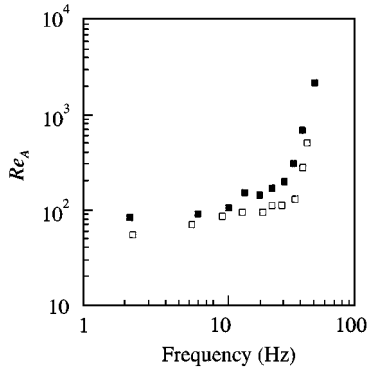


Figure 11. Acoustic Reynolds number $Re_A$ versus driving frequency for experiments with (■) and without (□) sidewall injection.

in $Re_A$ at approximately 15 Hz is caused by operating the wave generator at approximately one-third of the chamber's fundamental frequency. This setting excites the chamber's acoustic modes up to at least the sixth mode. Similarly, a small increase in $Re_A$ occurs at approximately 25 Hz due to the excitation of acoustic modes of the chamber as the wave generator is operated at approximately one-half of the chamber's fundamental frequency.

### 5.2. COMPARISON FOR A HARD WALL

When no dry ice is used, the experimentally measured amplitudes of acoustic oscillations recorded by the hot film match quite closely the theoretical values predicted from a one-dimensional, inviscid and irrotational acoustic solution in the chamber. This is to be expected since the flow can be considered to be inviscid everywhere except in the vicinity of the walls where a thin Stokes layer is formed. Hot-film measurements confirm that, outside of the Stokes layer, the motion in the so-called "outer region" can be well modelled by an inviscid and irrotational acoustic theory. In most test cases conducted, the Stokes boundary layer thickness was small. Viscous and rotational effects, including slight longitudinal velocity overshoot, were found to be insignificant outside the Stokes boundary layer.

### 5.3. COMPARISON FOR A TRANSPIRING WALL

For the case with dry ice, when sidewall injection of $CO_2$ is present, the experimentally measured amplitudes of acoustic oscillations recorded by the hot film are about one and a half times larger than the theoretical values predicted from a one-dimensional, inviscid and irrotational acoustic solution. This is to be expected since, when sidewall injection is present, the resulting boundary layer near the dry ice surface is significantly larger than before (without injection). This is captured experimentally by placing the hot film inside the Stokes boundary layer region. As shown by several researchers, including Flandro [14], and Majdalani [10, 11], a two-dimensional time-dependent field is more adequate to describe the flow velocity inside the laminar boundary layer. One important phenomenon exhibited by the velocity profile inside the boundary layer is the presence of a so-called Richardson overshoot near the wall [15]. This velocity augmentation is of a magnitude that is nearly twice the one-dimensional acoustic wave amplitude in the outer region. The overshoot is maximal near the wall where acoustic and vorticity wave amplitudes are additive when both

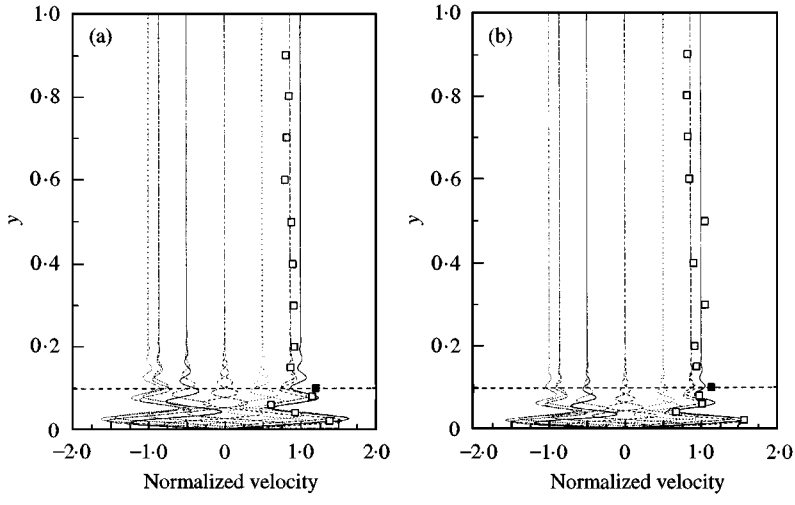


Figure 12. Comparison of experimental predictions [1–4] with theoretical timelines of the oscillatory velocity [11] near the dry ice surface. The horizontal line denotes the location of the hot film. For a $CO_2$ sublimation speed of $V = 0{\cdot}17$ m/s, viscosity $v = 1{\cdot}5 \times 1^{-5}$ m$^2$/s, and channel height $h = 76{\cdot}2$ mm, the frequency, Strouhal number ($\omega h/V$), and kinetic Reynolds number ($\omega h^2/v$) are (a) $f = 41{\cdot}2$ Hz, $Sr = 116$, $Re_k = 10^5$; and (b) $f = 50{\cdot}8$ Hz, $Sr = 143$, $Re_k = 1{\cdot}23 \times 10^5$. Measurements are denoted by (□) in general, and by (■) for the current location of the hot film. Evenly phased timelines correspond to $\omega t$: -·-·-·-·-·-, 0; —·—·—·—, $\pi/6$; ----, $\pi/3$; – – – –, $\pi/2$; ——, $2\pi/3$; -·-·-·-·-, $5\pi/6$; ·····, $\pi$; ---------, $7\pi/6$; ·····, $4\pi/3$; —·—·—·—, $3\pi/2$; · · · · · · ·, $5\pi/3$; – – – –, $11\pi/6$; ——, $2\pi$.

waves happen to be approximately in phase. This overshoot decays to one at the edge of the boundary layer where the vortical wave contribution becomes insignificant. The overshoot thus assumes a spatial average of 1·5 within the boundary layer. This theoretical average is in agreement with the average value recorded by the hot film.

When turbulence occurs, one may expect the boundary layer to be even thicker due to enhanced randomness and three dimensionality. Contrary to physical intuition, a time-averaged turbulent profile is characterized by a slight reduction in both overshoot and extension of the vorticity waves. Such results are consistent with the findings of Beddini *et al.* [16–18] and Yang *et al.* [19–21] who reported, with the onset of turbulence, vortical damping in both amplitude and penetration. The small discrepancy between our experimentally measured overshoot and that predicted theoretically by Majdalani [11] can be attributed, in most part, to the experimental error. This error stems from uncertainties in measuring the injection speed of $CO_2$, kinematic viscosity of the gas around the hot film, location of the hot film, and actual oscillation frequency. All of these parameters are needed to determine the exact amount of overshoot (see Majdalani [11] for a detailed discussion of the overshoot phenomenon). As shown in Figure 12, the experimentally measured amplitudes are larger than the one-dimensional wave amplitudes, and thus in agreement with current theories. Figure 13 gives the actual velocity and pressure traces from which the experimental amplitudes shown in Figure 12 were taken when the hot film was positioned 8 mm above the transpiring wall. In particular, when using the two-dimensional time-dependent solutions provided by Majdalani for a rectangular geometry [11], an excellent agreement is found to exist between analytical predictions and experimental results.

### 5.4. EXPERIMENTAL VERSUS THEORETICAL ACOUSTIC AMPLITUDES

The amplitude of the acoustic oscillation is determined by the net effects of the driving and damping mechanisms present in the system. The driving mechanism is the mechanical

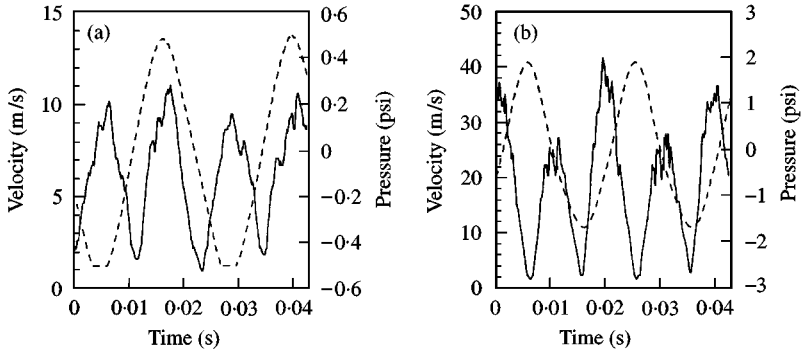


Figure 13. Velocity (——) and pressure (- - -) traces obtained from hot-film and pressure measurements. The hot film is located 10% (8 mm) above the transpiring walls (as in previous figure). The two cases correspond to (a) $f = 41{\cdot}2$ Hz and (b) $f = 50{\cdot}8$ Hz.

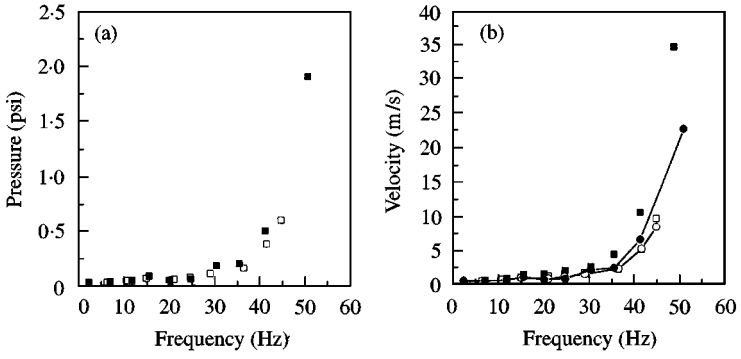


Figure 14. Measurements of (a) oscillating pressure amplitude and (b) oscillating velocity amplitude versus driving frequency for experiments with (■) and without (□) sidewall injection. For comparison, theoretical oscillating velocity amplitudes are also shown in (b) for physical settings with (–●–) and without (–○–) sidewall injection.

driving system which creates the acoustic oscillations. There are several known damping mechanisms. First, an energy sink is created because the seal between the dry ice and the flow chamber walls is not perfect. Also, the dry ice is a porous surface. As a pressure wave oscillates over a porous surface, the gas expands into the available surface pores which damps the pressure oscillations. Second, viscous effects are an energy sink which are expected to be greater for the case with dry ice than without dry ice because of the lower temperature and therefore lower viscosity with dry ice present. Third, flow turning, in this experiment, may be another energy sink. The sublimated gas from the solid $CO_2$ enters the flow field with a non-zero normal velocity component. Acoustic energy must therefore be transferred to the sublimating gas in order to increase the longitudinal velocity component at the expense of a normal velocity reduction. This is necessitated by the flow turning process which is accompanied by changes in flow directionality. Since the sublimation rate of dry ice has been observed to increase with increasing acoustic disturbance, the damping due to flow turning also increases with increasing acoustic disturbance.

Figure 14(a) shows the acoustic pressure amplitudes measured at the end of the flow chamber opposite the driving piston for the cases with and without dry ice in the test section. In both cases, the pressure amplitude increases with increasing driving frequency, as

predicted by acoustic theory. When the driving frequency approaches the fundamental frequency of the flow chamber, the pressure amplitude increases sharply. Acoustic theory predicts that pressure and velocity amplitudes will approach infinity at resonance, but this theory does not account for non-linearities and other acoustic damping factors. As a result, a small peak can be observed at 30.4 Hz for the case with dry ice. This small peak occurs because the acoustic modes of the flow chamber are excited by the harmonics of the driving piston.

The velocity amplitude as a function of driving frequency is shown in Figure 14(b) for the cases with and without dry ice in the test section. The velocity amplitude from acoustic theory using pressure amplitudes from the experiments is also shown. For both cases, the velocity amplitude increases with increasing driving frequency. As the driving frequency approaches the fundamental frequency of the flow chamber, the velocity amplitude increases sharply. Our experimental findings seem to be in good agreement with the theory.

## 6. CONCLUSIONS

Several experimental deficiencies of previous investigations were improved in this experiment. An experimental apparatus that incorporated a nearly pure harmonic wave generator has been successfully constructed and implemented. Undesirable harmonics produced by a typical slider-crank mechanism (used in previous experiments) have been minimized after substitution by a Scotch-yoke mechanism. Compared to former wave generators, the larger displacement volume of the Scotch-yoke has led to higher pressure amplitudes and, therefore, to higher sublimation rates. This negated the need for infrared heating lamps which were used previously to accelerate the sublimation process. The absence of an infrared lamp improved the accuracy of current measurements since it eliminated the interference of heat with hot-film signals.

A data-acquisition system controlled by a computer was implemented which was capable of collecting many samples of acoustic velocity and pressure data at consecutive cycles at the same driving frequency. The method of data collection facilitated statistical and spectral analysis of the acoustic data. This provided the means to later investigate the onset of turbulence for an oscillating flow in a channel with and without sidewall injection. Sidewall injection at the transpiring surface was achieved by using sublimating dry ice. Sublimating dry ice exhibited many desirable features such as (1) its ability to simulate the burning of a solid rocket propellant, (2) its non-interference with the natural system frequency, (3) its resistance to acoustic dissipation (through pores found in other traditional cold-flow experiments incorporating sidewall injection) and (4) its safe handling advantages.

Velocity measurements and fast Fourier transforms ascertained that the use of a Scotch-yoke mechanism is well suited to produce purely harmonic motions. As a result, accurate velocity measurements are successfully acquired and correlated. The experimental data sets furnished are unbiased, being the result of a purely harmonic driver.

The results show a velocity overshoot near the wall that is characteristic of oscillatory flows in general. This so-called Richardson velocity overshoot occurs near the wall whenever the phase difference is small between acoustic and vortical waves.

Comparisons to analytical predictions demonstrate a fair agreement with the current theory. In a sense, this investigation provides an experimental verification for the analytical formulation of the oscillatory velocity field in a rectangular channel with mean transmission of a transverse flow. This work also provides the means to carry out a straightforward characterization of turbulence. Conditions pertaining to the onset of turbulence are beyond the scope of this article and will be described in forthcoming work.

## REFERENCES


1. R. S. Brown, J. E. Erickson and W. R. Babcock 1974 *AIAA Journal* **12**, 1502–1510. Measuring the combustion response of a forced oscillation method.
2. R. S. Brown, A. M. Blackner, P. G. Willoughby and R. Dunlap 1986 *Journal of Propulsion and Power* **2**, 428–437. Coupling between acoustic velocity oscillations and solid propellant combustion.
3. R. S. Brown, A. M. Blackner, P. G. Willoughby and R. Dunlap 1986 *AIAA Paper No.* 86-0531, *January*, Coupling between velocity oscillations and solid propellant combustion.
4. C. W. Shaeffer and R. S. Brown 1992 *Chemical Systems Div. Technical Report No.* 2060 *FR*, *United Technologies*, *San Jose*, *CA*. Oscillatory internal flow studies.
5. F. E. C. Culick 1966 *AIAA Journal* **4**, 1462–1464. Rotational axisymmetric mean flow and damping of acoustic waves in a solid propellant rocket.
6. Y. Ma, W. K. Van Moorhem and R. W. Shorthill 1989 *Combustion Instabilities Driven by Thermo-Chemical Acoustic Sources*. vol. 5. NCA **4**, HTD **128**, 17–22. New York: American Society of Mechanical Engineers. Innovative method of investigating the role of turbulence in the velocity coupling phenomenon.
7. Y. Ma 1990 *Ph.D. Thesis*, *University of Utah*, *Salt Lake City*. A simulation of the flow near a burning propellant in a solid propellant rocket motor.
8. Y. Ma, W. K. Van Moorhem and R. W. Shorthill 1990 *Journal of Vibration & Acoustics—Transactions of the ASME* **112**, 550–555. Innovative method of investigating the role of turbulence in the velocity coupling phenomenon.
9. Y. Ma, W. K. Van Moorhem and R. W. Shorthill 1991 *Journal of Propulsion and Power* **7**, 692–699. Experimental investigation of velocity coupling in combustion instability.
10. J. Majdalani 1995 *Ph.D. Thesis*, *University of Utah*, *Salt Lake City*, *UT*. Improved flowfield models in rocket motors and the Stokes layer with sidewall injection.
11. J. Majdalani 1999 *Journal of Sound and Vibration* **223**, 73–95. Asymptotic formulation for an acoustically driven field inside a rectangular cavity with a well-defined convective mean flow motion.
12. H. Schlichting 1979 *Boundary-Layer Theory*. New York: McGraw-Hill Book Company Inc., seventh Edition.
13. G. G. Stokes 1847 *Transactions of the Cambridge Philosophical Society* **8**, 441–455. On the theory of oscillatory waves.
14. G. A. Flandro 1989 *Combustion Instabilities Driven by Thermo-Chemical Acoustic Sources*, vol. 5. NCA **4**, HTD **128**, 53–61, New York: American Society of Mechanical Engineers. Effects of vorticity transport on axial acoustic waves in a solid propellant rocket chamber.
15. E. G. Richardson and E. Tyler 1929 *Proceedings of the Royal Society*, *London* **A 42**, 1–15. The transverse velocity gradient near the mouths of pipes in which an alternating or continuous flow of air is established.
16. R. A. Beddini 1986 *AIAA Journal* **24**, 1766–1773. Injection-induced flows in porous-walled ducts.
17. R. A. Beddini and T. A. Roberts 1988 *AIAA Journal* **26**, 917–923. Turbularization of an acoustic boundary layer on a transpiring surface.
18. R. A. Beddini and T. A. Roberts 1992 *Journal of Propulsion and Power* **8**, 290–296. Response of propellant combustion to a turbulent acoustic boundary layer.
19. D. L. Cherng, V. Yang and K. K. Kuo 1989 *Journal of Propulsion and Power* **5**, 678–685. Numerical study of turbulent reacting flows in solid-propellant ducted rocket combustors.
20. T. A. Jarymowycz, V. Yang and K. K. Kuo 1992 *Journal of Propulsion and Power* **8**, 346–353. Numerical study of solid-fuel combustion under supersonic crossflows.
21. I. S. Tseng and V. Yang 1994 *Combustion & Flame* **96**, 325–342. Combustion of a double-base homogeneous propellant in a rocket motor.